ANTIOXIDANTS & REDOX SIGNALING
Volume 10, Number 10, 2008

DOI: 10.1089/ars.2007.1999

Original Research Communication

Advanced Oxidation Protein Products Activate Vascular Endothelial Cells *via* a RAGE-Mediated Signaling Pathway

Zhi Jian Guo,[1] Hong Xin Niu,[1] Fan Fan Hou,[1] Lu Zhang,[1] Ning Fu,[2] Ryoji Nagai,[4] Xiao Lu,[2] Bai Hong Chen,[3] Yue Xin Shan,[1] Jian Wei Tian,[1] Ram H. Nagaraj,[5] Di Xie,[1] and Xun Zhang[1]

Abstract

The accumulation of advanced oxidation protein products (AOPPs) has been linked to vascular lesions in diabetes, chronic renal insufficiency, and atherosclerosis. However, the signaling pathway involved in AOPPs-induced endothelial cells (ECs) perturbation is unknown and was investigated. AOPPs modified human serum albumin (AOPPs-HSA) bound to the receptor for advanced glycation end products (RAGE) in a dose-dependent and saturable manner. AOPPs-HSA competitively inhibited the binding of soluble RAGE (sRAGE) with its preferential ligands advanced glycation end products (AGEs). Incubation of AOPPs, either prepared *in vitro* or isolated from uremic serum, with human umbilical vein ECs induced superoxide generation, activation of NAD(P)H oxidase, ERK 1/2 and p38, and nuclear translocation of NF-κB. Activation of signaling pathway by AOPPs-ECs interaction resulted in overexpression of VCAM-1 and ICAM-1 at both gene and protein levels. This AOPPs-triggered biochemical cascade in ECs was prevented by blocking RAGE with either anti-RAGE IgG or excess sRAGE, but was not affected by the neutralizing anti-AGEs IgG. These data suggested that AOPPs might be new ligands of endothelial RAGE. AOPPs-HSA activates vascular ECs *via* RAGE-mediated signals. *Antioxid. Redox Signal.* 10, 1699–1712.

Introduction

Accelerated atherosclerosis and vascular disease are the major complications of diabetes and chronic renal insufficiency, constituting the leading cause of morbidity and mortality in these ubiquitous disorders (11, 18, 27). Many underlying factors could contribute to this outcome, including abnormalities in lipid metabolism, hypertension, and renal dysfunction. Diabetes and renal insufficiency are associated with increased modification of protein. Numerous studies have demonstrated that the formation and accumulation of advanced glycation end products (AGEs), the products of nonenzymatic glycation/oxidation of proteins/lipids, induce vascular perturbation mainly through interaction of AGEs with the cell surface receptor for AGEs (RAGE) (46).

In addition to AGEs, a newly identified family of oxidized protein compounds, termed advanced oxidation protein products (AOPPs), has emerged as novel mediators of inflammation. AOPPs are the dityrosine-containing and cross-linking protein products which were first isolated from uremic plasma (43). Accumulation of AOPPs was subsequently found in patients with diabetes (15) and coronary artery disease (8, 16), as well as subjects with obesity (3). AOPPs can be formed *in vitro* by exposure of serum albumin to hypochlorous acid (HOCl). *In vivo*, plasma AOPPs are mainly carried by albumin, and their concentrations are closely correlated with the levels of dityrosine (6, 43). Therefore, AOPPs have been considered as novel markers of oxidative stress (43).

Our recent study demonstrated that intravenous infusion of AOPPs–albumin significantly increases macrophage infil-

[1]Division of Nephrology, Nanfang Hospital; and Departments of [2]Immunology and [3]Biological Technique, Southern Medical University, Guangzhou, China; [4]Department of Medical Biochemistry, Graduate School of Medical and Pharmaceutical Sciences, Kumamoto University, Japan; [5]Department of Ophthalmology, Center for Vision Research, Case Western Reserve University and University Hospital of Cleveland, Ohio.

tration in atherosclerotic plaques in hypercholesterolemic rabbits (24) and in glomeruli in the remnant kidney model (20), suggesting that AOPPs are not only the markers of oxidative stress, but potential inducers of vascular inflammation. Consistent with the observation, accumulation of AOPPs has been found in both experimental and human atherosclerotic lesions (9, 24) and has been linked to endothelial cells (ECs) dysfunction and monocyte activation (26, 44).

Although these reports support a role for AOPPs in mediating vascular cellular perturbation, the molecular basis of proinflammatory effect of AOPPs remains largely unknown. It is still not clear whether AOPPs induce ECs perturbation by receptor-mediated mechanisms, and, if it is the case, what receptor(s) might be involved in this pathway. Moreover, the intracellular signal transduction processes triggered by AOPPs have not been well understood.

In this study, we focused on elucidating the receptor and the signaling pathway activated by AOPPs–albumin in human ECs. Our data demonstrated that AOPPs, as a class of new ligand of RAGE, activated vascular ECs through a RAGE-mediated signals involving PKC, NAD(P)H oxidase, ERK1/2, p38, and nuclear transcription factor κB (NF-κB). These data provide new insight on how AOPPs might prime vascular inflammation in diverse disorders such as diabetes, chronic renal insufficiency, and atherosclerosis.

Materials and Methods

Cell culture

Human umbilical vein endothelial cells (HUVECs) were prepared and cultured as described (13). The experiment utilized confluent cultures grown in RPMI 1640 (HyClone, Logan, Utah) and pooled, heat-inactivated human group AB serum (20%). Only first-passage cells from one umbilical cord were used for one experiment.

AOPPs and AGEs preparation

AOPPs–human serum albumin (HSA) was prepared *in vitro* as described previously (44). Briefly, fatty acid-free HSA (Sigma, St. Louis, MO) was exposed to 200 mmol/L HOCl (Fluke, Buchs, Switzerland) for 30 min in the absence of free amino acid/carbohydrate/lipids to exclude formation of AGEs-like structures. The preparation was dialyzed overnight against PBS to remove free HOCl.

To prepare high-molecular-weight AOPPs fraction (AOPPs-F) formed *in vivo* (43), serum was isolated from patients with uremia. AOPPs-F was prepared by using HiPrep 16/60 Sephacryl S-300 HR column (GE Healthcare Bio-Sciences AB, Uppsala, Sweden) according to the manufacturer's protocol. The concentration of AOPPs-F in patient's serum, calculated by total protein amount of AOPPs-F/serum sample volume, was ~200 μg/ml. The collected AOPPs-F was concentrated 100 times by Amicon Ultra-15 centrifugal filter devices (Millipore Corporation, Billerica, MA).

To remove AGEs likely contained in the serum, the prepared AOPPs-F was passed through an anti-AGEs IgG immobilized Affi-Gel 10 column (BioRad Hercules, CA) as described (45). The material that did not adhere to this column was used for the experiments. Samples were also passed through a Detoxi-Gel column (Pierce, Rockford, IL) to remove any contaminated endotoxin. Endotoxin levels in the preparation were determined with the amebocyte lysate assay kit (Sigma) and were found to be below 0.025 EU/ml.

AOPPs content in the preparation was determined as described previously (44). The content of AOPPs was 72.4 $\pm$ 9.8 nmol/mg protein in prepared AOPPs-HSA, 52.6 $\pm$ 7.6 nmol/mg protein in isolated AOPPs-F, and 0.2 $\pm$ 0.02 nmol/mg protein in native HSA. The components of AGEs, including N^{ε}-(carboxylmethyl) lysine (CML), pentosidine, pyridine (12, 24, 28), and glyoxal-, glycolaldehyde-, and glyceraldehyde-modified proteins (14, 33), were determined as described and were found to be undetectable in the prepared samples.

AGEs-HSA was prepared as described previously by incubating HSA with 0.15 *M* glyoxylic acid (CML-HSA) (32), 50 m*M* glycolaldehyde dimmer (GA-HSA) (39), 500 m*M* ribose (RB-HSA) (39), 100 m*M* glyceraldehyde (GC-HSA)(33), separately.

ROS production

The levels of intracellular reactive oxygen species (ROS) were determined by measuring the fluorescence of 5 (and 6)-chloromethyl-2′, 7′-dichlorodrofluorescein diacetate (DCF, Molecular Probe, Carlsbad, CA) (4). Briefly, HUVECs were pre-incubated for 30 min with 1 nmol/L DCF in PBS lacking Ca^{2+} and Mg^{2+}. The cells were then incubated with various concentrations of AOPPs-HSA for indicated times or with 200 μg/ml of AOPPs-F for 30 min. One milliter aliquots of the cells were removed for fluorescence intensity analysis on a flow cytometry (BD FACSCalibur system, Franklin Lakes, NJ). To verify the sources of ROS generation, HUVECs were pre-incubated for 10 min with NAD(P)H oxidase inhibitors (*i.e.*, diphenyleneiodonium, DPI, 10~100 μmol/L; apocynin, 5~500 μmol/L), a nitric oxide synthase inhibitor (N^{G}-nitro-L-arginine methyl ester, L-NAME, 100~1000 μmol/L), a xanthine oxidase inhibitor (oxypurinol, 10~100 μmol/L), a mitochondria inhibitor (rotenone, 2.5~250 μmol/L), an inhibitor of protein kinase C (PKC) (Gö6983, 1 μ*M*) and a O_2^-scavenger that can enter the cells and reduces intracellular ROS (7) (bovine cytosolic Cu/Zn SOD, c-SOD 2~200 u/ml) (all from Sigma). The experiments were then repeated as described above.

To further confirm the intracellular source of ROS, NAD(P)H-dependent O_2^- production was assessed by lucigenin-enhanced chemiluminescence as described previously (21). Cell homogenates (100 μg/well) were added into a 96-well microplate. Immediately before recording, dark-adapted lucigenin (5 μmol/L) with or without NAD(P)H (100 μmol/L) were added to cell homogenates. Light emission was recorded every minute for 30 min (VICTOR V Wallac 1420, PerkinElmer, Turku, Finland). Data were expressed as counts per second (CPS). To verify NAD(P)H oxidase contribution, the procedure was repeated in the presence of DPI, apocynin, L-NAME, oxypurinol, rotenone, Gö 6983, and c-SOD.

Effect of AOPPs–RAGE interaction on ROS generation

Binding of AOPPs to RAGE. The binding activity of AOPPs-HSA to the extracellular domain of RAGE (sRAGE) was determined using a microplate-based assay as described (39). Briefly, microtiter wells (Corning, Lowell, MA) were coated with 10 μg/ml of AOPPs-HSA, AGEs-HSA, or native

HSA overnight at 4°C. After washing and blocking, the wells were incubated with indicated concentrations of sRAGE (47) for 30 min at 37°C. The bound sRAGE was detected with a horseradish peroxidase (HRP)-conjugated monoclonal anti-RAGE IgG (47) and measured by a microplate reader (Bio-Rad, Hercules, CA).

As an alternative approach, CML-HSA (10 μg/ml) was immobilized onto the wells. sRAGE (4 μg/ml) was pre-incubated with indicated concentrations of AOPPs-HSA, CML-HSA, GA-HSA, or native HSA for 30 min at 37°C and then added to the wells. The binding of sRAGE with immobilized AGEs-HSA was quantified by the anti-RAGE IgG as described above.

ROS generation under blocking of AOPPs–RAGE interaction

HUVECs were pre-incubated with a rabbit anti-RAGE IgG (R&D System, Minneapolis, MN), nonimmune rabbit IgG (Santa Cruz Biotechnology, Inc., Santa Cruz, CA), or excess sRAGE for 2 h at 37°C. The cells were washed and incubated with 200 μg/ml of AOPPs-HSA or native HSA for 30 min at 37°C. ROS generation was quantified by measuring the DCF fluorescence as described above.

To further exclude the effect of AGEs contamination, 200 μg/ml of AOPPs-HSA was pre-incubated for 30 min with a neutralizing anti-AOPPs (prepared by Department of Immunology, Southern Medical University), or with neutralizing anti-AGEs antibodies such as 6D12 (17) and anti-GXL (33) at concentrations that could neutralize the AGEs–cell interaction. The treated AOPPs were then incubated with ECs, and ROS production was quantified as described above.

Detection of NAD(P)H oxidase activation

P47^{phox} phosphorylation. Phosphorylation of p47^{phox} was detected by immunoprecipitation as described previously (36). Briefly, the cell lysates were pre-absorbed with protein A/G agarose beads (Santa Cruz Biotechnology) at 4°C for 30 min. The supernatants were incubated with a rabbit anti-human p47^{phox} polyclonal antibody (Upstate-Cell Signaling Solutions, Temecula, CA) overnight at 4°C. The immunocomplexes were resolved with SDS-PAGE, and transferred to nitrocellulose membranes (Amersham Pharmacia Biotech, Piscataway, NJ). The membranes were then incubated with a HRP-conjugated rabbit anti-phosphoserine antibody (Stressgen Bioreagents Corp. Victoria, BC, Canada) and were detected with ECL (Pierce). To determine pan-p47^{phox}, the membranes were washed with an elute buffer, reacted with a mouse anti-human p47^{phox} monoclonal antibody (BD Biosciences Pharmingen, San Diego, CA), and subsequently detected with HRP-conjugated rabbit anti-mouse IgG (DakoCytomation, Glostrup, Denmark) and ECL. Bands were quantified by a densitometry (Universal Hood. 2, BioRad, Milan, Italy), and values for phospho-p47^{phox} expression were normalized to the amount of total p47^{phox} per sample.

Interaction of p47^{phox} with p22^{phox} and Nox homologues

The interaction of p47^{phox} with p22^{phox} and Nox homologues was analyzed by immunoblotting as described previously (22). The immunocomplexes were obtained by incubation of cell lysates with the rabbit anti-human p22^{phox}, Nox 2, or Nox 4 polyclonal antibodies (Santa Cruz Biotechnology) overnight at 4°C, separately. Immunoblotting was performed using the mouse anti-human p47^{phox} monoclonal antibody as the primary antibody and the HRP-conjugated rabbit anti-mouse IgG as the secondary antibody. The membranes were detected by ECL. To determine the total p22^{phox}, Nox 2, and Nox 4, the membranes were eluted and incubated with the rabbit anti-human p22^{phox}, Nox 2, or Nox 4 polyclonal antibodies and then detected by reaction with the HRP-linked anti-rabbit IgG (Cell Signaling Technology, Beverly, MA).

P47^{phox} membrane translocation

HUVECs were fixed in acetone-methanol (1:1, [vol/vol]). After washing and blocking, the cells were incubated with a mouse anti-human p47^{phox} monoclonal antibody overnight at 4°C. After washing, the slides were incubated with a FITC-conjugated rabbit anti-mouse immunoglobulins (DakoCytomation) for 45 min at 37°C, washed, stained with propidium iodide (PI, Sigma) and observed under a confocal microscopy (Leica TCS SP2 AOBS, Leica Microsystems, Cambridge, UK).

Detection of MAPK activation

HUVECs were stimulated with AOPPs-HSA as described above. In some experiments, cells were pre-incubated for 1 h at 37°C with the following inhibitors: c-SOD, apocynin, U0126 (a ERK1/2 inhibitor, Cell Signaling Technology) and SB203580 (a p38^{MAPK} inhibitor, Promega, Madison, WI). MAPK activation was detected as described (36). Cell homogenates (40 μg protein in each sample) were immunoblotted using the rabbit polyclonal antibodies against human pan- or phospho-ERK1/2, p38^{MAPK}, and JNK1/2 as the primary antibodies, and a HRP-linked anti-rabbit IgG as the secondary antibody (all from Cell Signaling Technology). Bands were quantified by a densitometry and values for phospho-MAPK expression were normalized to the amount of total MAPK per sample.

Detection of NF-κB activation

Western blot analysis. HUVECs were incubated with 200 μg/ml of AOPPs-HSA for 15~120 min or with native HSA for 30 min. In some experiments, cells were pretreated with SN50 (a NF-κB inhibitor, Alexis Biochemicals, San Diego, CA) or apocynin, U0126 and SB203580 for 1 h at 37°C, and then stimulated with AOPPs-HSA for 30 min. NF-κB p65 in cells lysates were measured by Western blot analysis as described previously by using rabbit anti-human NF-κB/p65 (BioVision, Mountain View, CA) as the primary antibody (48).

Immunofluorescence. NF-κB nuclear translocation was also determined by immunofluorescence staining as described (23). HUVECs were rinsed and fixed with actone-methanol (1:1 [vol/vol]) at −20°C for 10 min. The slides were blocked in 1% BSA, incubated with a rabbit anti-human NF-κB/p65 antibody overnight at 4°C, and reacted with a FITC-conjugated swine anti-rabbit immunoglobulins for 45 min at 37°C. The slides were stained with PI and observed under the confocal microscopy.

EMSA. Nuclear protein extracts of HUVECs were prepared as described above. The probe for NF-κB EMSA was a double-stranded oligonucleotide (5′AGT TGA GGG GAC TTT CCC AGG C 3′; 3′TCA ACT CCC CTG AAA GGG TCC G 5′, Promega). EMSA was performed using Dig Gel Shift Kit (Roche Applied Science, Mannheim, Germany) according to the manufacturer's protocol. In competition analysis, nuclear extracts were incubated with 125X unlabeled oligonucleotide probes of both NF-κB and control factor Oct2A for 1 h before the addition of labeled oligonucleotides. For supershift analysis, a rabbit anti-human NF-κB/p65 and an anti-human NF-κB/p50 (Santa Cruz Biotechnology) were added to the reaction mixture 12 h before the addition of labeled oligonucleotides at 4°C.

Detection of VCAM-1 and ICAM-1 expression

Real time PCR. Total RNA was prepared using the RNA extraction kit with DNase I treatment following the manufacturer's instructions (Promega). To generate cDNA, total RNA (1 μg) from each of triplicate samples was mixed and converted into cDNA using random primers and the Rever-Tra Ace -α-™ First Strand cDNA Synthesis Kit (Toyobo Co., Ltd., Osaka, Japan). All cDNA samples were aliquoted and stored at −80°C. Primers were designed using the Primer Express oligo design software (Applied BioSystems, Foster City, CA) and synthesized by Invitrogen (Carlsbad, CA). All primer sets were subjected to rigorous database searches to identify potential conflicting transcript matches to pseudogenes or homologous domains within related genes. The sequences of the real-time PCR primers are as follows: human ICAM-1: sense 5′-GCAATGTGCAAGAAGATAGCCA-3′, antisense 5′-CCCGTTCTGGAGTCCAGTACAC-3′; human VCAM-1: sense 5′-GAATTGCAAGTCTACATATCACCCA-3′, antisense 5′-TCGCTGGAACAGGTCATGG-3′; β-actin: sense 5′-AAGATCATTGCTCCTCCTGAGC-3′, antisense 5′-TCCTGCTTGCTGATCCACATC-3′. The SYBR Green I assay and the MX 3005P thermocycler (Stratagene, La Jolla, CA) were used for detecting the products from the reverse-transcribed cDNA samples. β-Actin was used as the normalizer. PCR reactions for each sample were performed in duplicate, and the relative gene expressions were analyzed as described previously (25).

Western blot analysis. HUVECs were lysed, resolved with SDS-PAGE, and transferred to nitrocellulose membranes as described (36). After blocking, the membranes were incubated with the rabbit anti-human ICAM-1 or VCAM-1 antibodies (Santa Cruz Biotechnology), reacted with the HRP-linked anti-rabbit IgG, and detected by ECL.

To determine whether AOPPs take effect through ligation of RAGE, the cells were pre-incubated for 2 h at 37°C with the following blocking antibodies against known AGEs binding proteins (10) : rabbit anti-human RAGE (10∼100 μg/ml), rabbit anti-AGEs receptor 1 (AGE-R1, 1:100∼1:20), AGEs receptor 2 (AGE-R2 , 1:100∼1:20) and AGEs receptor 3 (AGE-R3, 1:100∼1:20) (kindly provided by Prof. Hellen Vlassara, Division of Experimental Diabetes and Aging, Mount Sinai School of Medicine, New York), goat anti-human scavenger receptor class A type 1 (SR-AI, 2∼100 μg/ml, R&D Systems), rabbit anti-human scavenger receptor class B type 1 (SR-BI, 20∼100 μg/ml, Abcam, Cambridge, UK), monoclonal anti-human CD36 (2∼100 μg/ml, Cayman Chemical, Ann Arbor, MI), goat anti-human lectin-like oxidized low-density lipoprotein receptor-1/ scavenger receptor class E type 1 (LOX-1/SR-E1, 10∼100 μg/ml, R&D Systems), goat anti-human scavenger receptor expressed by ECs/ scavenger receptor class F type 1 (SREC-I/SR-F1, 0.5∼5 μg/ml, R&D Systems). The cells were then incubated with AOPPs-HSA or AOPPs-F for 12 h. Expression of ICAM-1 and VCAM-1 was measured as described above.

Immunostaining. Immunostaining for ICAM-1 and VCAM-1 was performed as described previously (23). Cells cultured were fixed with acetone-methanol (1:1), blocked with 1% BSA, incubated with rabbit anti-human ICAM-1 or VCAM-1 antibodies, and reacted with a FITC-conjugated swine anti-rabbit immunoglobulin. The slides were observed under the confocal microscopy after staining with PI.

Statistical Analysis

All experiments were performed in triplicate. Continuous variables, expressed as mean ± SEM, were compared using one-way ANOVA or Welch method when the assumption of equal variances did not hold. Pairwise comparisons were evaluated by the Student–Newman–Keuls procedure or Dunnett's T3 procedure when the assumption of equal variances did not hold. The Dunnett procedure was used for comparisons between reference group and other groups. Two-tailed P values, 0.05 were considered statistically significant. Statistical analyses were conducted with SPSS 13.0 by Department of Biostatictics, Southern Medical University.

Results

AOPPs induced ROS production in ECs

ROS production, as determined by fluorescence of DCF, was significantly increased by exposure of HUVECs with AOPPs-HSA in a dose- (Fig. 1A) and time-dependent (Fig. 1B) manner. Exposure of HUVECs to native HSA did not induce ROS generation (Fig. 1A).

To verify the enzymatic sources of ROS generation, HUVECs were pretreated with the inhibitors of various en-

FIG. 1. AOPPs-induced ROS production. (**A**) ROS production detected by DCF fluorescence in HUVECs stimulated by indicated concentrations of AOPPs-HSA, AOPPs-F or native HSA. (**B**) Time course of AOPPs-HSA (200 μg/ml)-induced ROS production. (**C**) AOPPs-induced ROS generation in HUVECs pretreated with apocynin, DPI, L-NAME, rotenone, oxypurinol, c-SOD, or Gö6983. (**D**) NAD(P)H-dependent O_2^- generation determined by lucigenin-enhanced chemiluminescence in HUVECs homogenates. (**E**) Time course of AOPPs-HSA (200 μg/ml)-induced O_2^- production. (**F**) AOPPs-HSA-induced enhancement of O_2^- production was markedly attenuated by pretreating the cells with apocynin, DPI and Gö6983. Data from three independent experiments are shown as mean ± SEM. ANOVA, $p < 0.001$ in **A**, **B**, **C**, **D**, **E**, and **F**; *$p < 0.05$ *vs.* HSA group; #$p < 0.05$ *vs.* group without respective inhibitors.

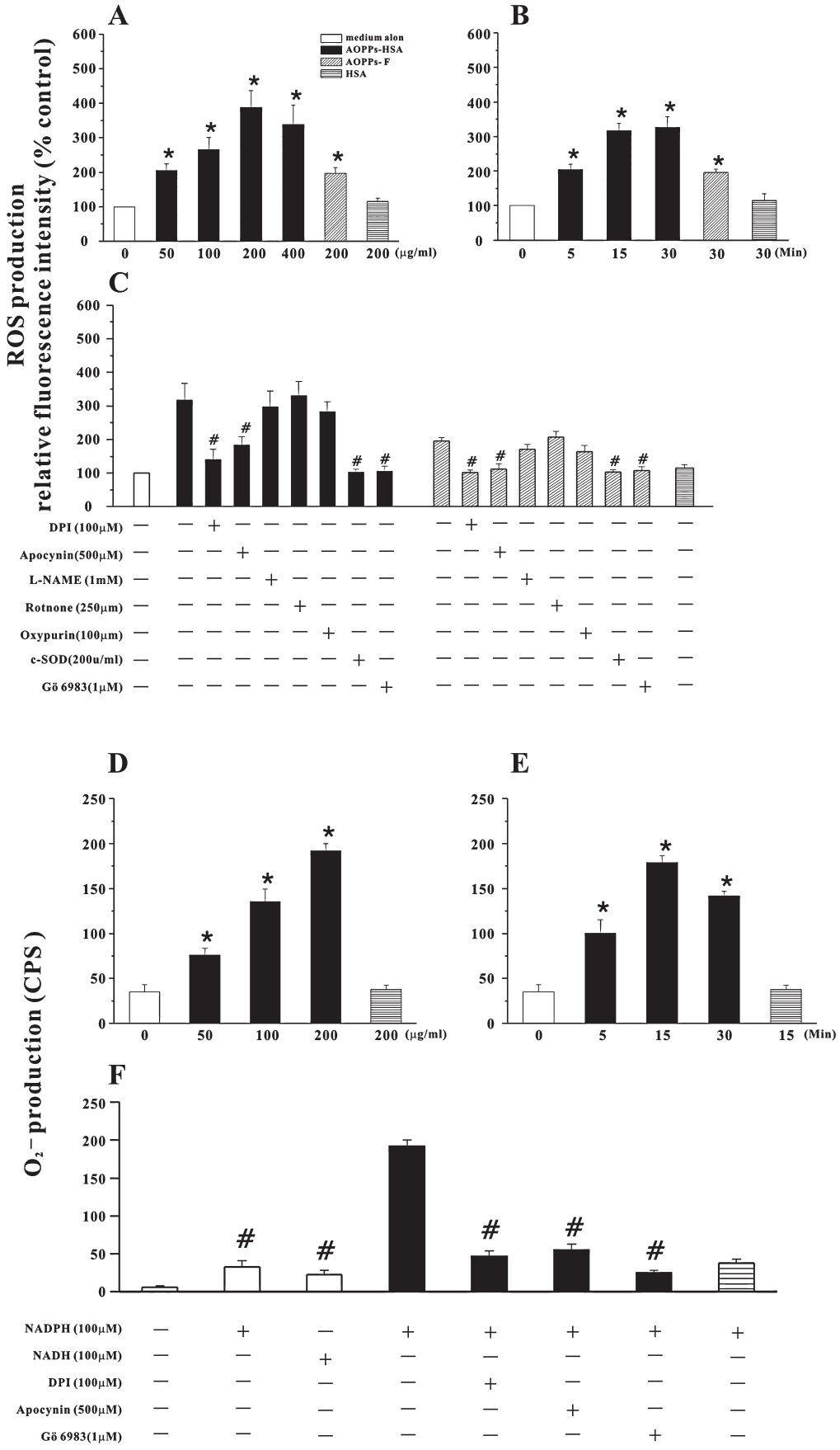
A
B
C
D
E
F
ROS production
relative fluorescence intensity (% control)
medium alon
AOPPs-HSA
AOPPs- F
HSA
(μg/ml)
(Min)
DPI (100μM)
Apocynin(500μM)
L-NAME (1mM)
Rotnone (250μm)
Oxypurin(100μm)
c-SOD(200u/ml)
Gö 6983(1μM)
O2 – production (CPS)
NADPH (100μM)
NADH (100μM)

FIG. 1.

zymatic systems involved in ROS generation (Fig. 1C). AOPPs-HSA-induced ROS production was significantly suppressed (by 79.8 ± 15.1% and 60.3 ± 13.9%, mean ± SEM) by the NAD(P)H oxidase inhibitors DPI and apocynin, but not by a inhibitor of nitric oxide synthase, a xanthine oxidase inhibitor, and a mitochondria inhibitor, suggesting that NAD(P)H oxidase played a central role in AOPPs-induced ROS production. Similarly, the exposure of HUVECs to AOPPs-F increased ROS generation (Fig. 1A) that was suppressed by NAD(P)H oxidase inhibitors (Fig. 1C).

To further confirm the intracellular source of ROS, NAD(P)H-dependent O_2^- production in HUVECs was examined by lucigenin-enhanced chemiluminescence. In the absence of added NAD(P)H, there was no detectable O_2^- production in HUVECs. However, in the presence of exogenous NAD(P)H, O_2^- production was significantly increased in cells stimulated by AOPPs-HSA as compared with unstimulated HUVECs or cells pre-stimulated by native HSA (Fig. 1D, E, and F). O_2^- production was significantly inhibited by pretreating the cells with NAD(P)H oxidase inhibitors, consistent with NAD(P)H oxidase as the major source. The inhibitors alone, at the concentration used in the experiments, had no significant effect on ROS or O_2^- generation in cells treated with medium alone (data not shown).

ROS or O_2^- production induced by AOPPs could by completely blocked by a broad spectrum PKC inhibitor, suggesting that PKC activation might be the necessary upstream event of AOPPs-triggered intracellular oxidative stress.

ROS Production was dependent on interaction of AOPPs with RAGE

Previous studies have demonstrated that ligation of the cell surface receptor RAGE triggers intracellular oxidant stress (19). RAGE is a multiligand receptor and expresses on ECs (46). Therefore, we examined whether AOPPs triggered ROS production by engagement of RAGE. AOPPs-HSA, CML-HSA, GA-HSA, and native HSA were coated onto the microwells and incubated with indicated concentrations of sRAGE. The binding capacity of sRAGE to immobilized AOPPs-HSA increased as a function of sRAGE concentrations and in a saturable manner (Fig. 2A). Moreover, AOPPs-HSA inhibited sRAGE binding to immobilized CML-HSA in a dose-dependent manner (Fig. 2B). The binding affinity of AOPPs-HSA to sRAGE was significantly higher than that of CML-HSA and lower than that of GA-HSA at the equal molar concentrations. (Fig. 2B).

We next tested whether AOPPs-induced ROS generation was dependent on RAGE. Pretreatment of HUVECs with anti-RAGE IgG or excess sRAGE blocked ROS generation in a dose-dependent manner (Fig. 2C). In contrast, nonimmune IgG (Fig. 2C) or excess concentrations of albumin had no effect (data not shown).

To further confirm that ROS generation was not induced by AGEs contamination, the neutralizing experiments were conducted using specific antibodies against AOPPs, CML, GA-, GC-, and ribose (RB)-derived AGEs, separately. ROS generation induced by AOPPs could be inhibited by the anti-AOPPs antibody that did not recognize HSA, CML-, GA-, GC-, and RB-derived AGEs (Fig. 2D). ROS generation triggered by AOPPs could not be inhibited by 6D12 which neutralize CML, GA- and GC-derived AGEs (17) (Figs. 2E and F). Furthermore, anti-GXL (33), a neutralizing antibody recognize RB- and GC-derived proteins, had no effect on AOPPs-induced ROS production (data not shown).

AOPPs-HSA activated ECs NAD(P)H oxidase through ligation of RAGE

To further investigate the mechanisms underlying the induction of ROS by AOPPs-HSA, we examined the effect of AOPPs-HSA on ECs NAD(P)H oxidase. AOPPs-HSA or AOPPs-F induced rapid $p47^{phox}$ phosphorylation at 5 min and peaking at ~15 min. Native HSA had no effect (Fig. 3A). AOPPs-induced $p47^{phox}$ phosphorylation could be blocked by pretreatment of HUVECs with anti-RAGE IgG or a broad spectrum PKC inhibitor (Fig. 3A), but not by nonimmune IgG (Fig. 3A) or pretreatment of AOPPs with anti-AGEs antibodies (anti-CML, 6D12, and anti-GXL) (data not shown).

To examine the interaction of $p47^{phox}$ with $p22^{phox}$ and Nox homologues, we immunoprecipitated $p22^{Phox}$, Nox 2, and Nox 4 with the specific antibodies, and then probed for the co-existence of $p47^{phox}$. As shown in Fig. 3B, the amount of $p47^{phox}$–$p22^{phox}$ complex formation rapidly increased in AOPPs-stimulated HUVECs. AOPPs promoted the association of $p47^{phox}$ with both Nox 2 and Nox 4 (Figs 3C and D). At 15 min after AOPPs challenge, $p47^{phox}$ membrane translocation was apparent (Fig. 3E).

AOPPs activated ERK 1/2 and $P38^{MAPK}$ mainly through NAD(P)H oxidase-dependent O_2^- generation

To determine whether interaction of AOPPs with RAGE triggers MAPK signaling, MAPK activity was evaluated in the presence or absence of AOPPs-HSA. In native HSA-treated cells, there were very low levels of phospho-ERK 1/2 and phospho-$p38^{MAPK}$ (Figs. 4D and E) and almost no detectable phospho-JNK 1/2. AOPPs-HSA induced a rapid phosphorylation of ERK 1/2 and $p38^{MAPK}$ (Figs. 4A and B), but had no effect on JNK (Fig. 4C). The specificity of AOPPs-induced activation of ERK 1/2 or $p38^{MAPK}$ was further confirmed by the inhibitable phosphorylation in cells pretreated with U0126 or SB 203580 (Figs. 4D and E).

To determine whether ERK 1/2 and $p38^{MAPK}$ activation was attributable to RAGE-mediated, NAD(P)H oxidase-dependent O_2^- generation, we treated HUVECs with the anti-RAGE IgG, c-SOD, or apocynin. Anti-RAGE IgG, but not nonimmune IgG, blocked the AOPPs-HSA-induced activation of ERK 1/2 and $p38^{MAPK}$. Apocynin and c-SOD significantly inhibited the activation of ERK 1/2 (by 79.89 ± 11.38% and 84.18 ± 11.66%) and $p38^{MAPK}$ (by 79.96 ± 7.76% and 83.33 ± 5.67%) (Figs. 4D and E). These data suggested that MAPK activation was mediated by interaction of AOPPs with RAGE and regulated by O_2^- generated by NAD(P)H oxidase activation.

AOPPs activated NF-κB through RAGE-mediated signals

Compared with native HSA, stimulation of HUVECs with AOPPs-HSA significantly increased the translocation of p65 from the cytosol to the nucleus (Figs. 5A–C). This was blocked by pretreatment of cells with the NF-κB inhibitor, SN50 (Fig. 5D). The supershift assay using specific antibodies against p65 and p50 suggested that the AOPPs-induced

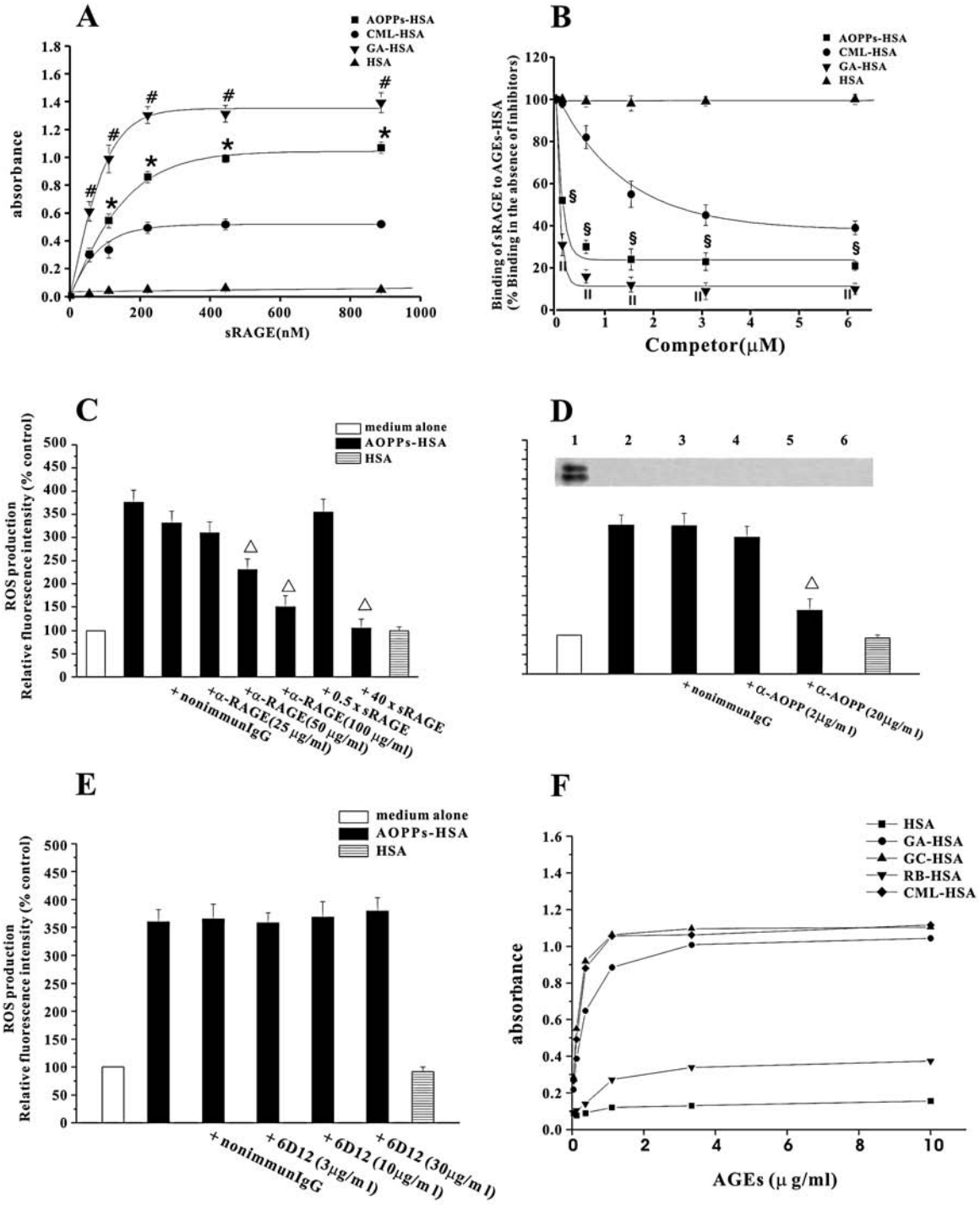

FIG. 2. Interaction of AOPPs-HSA with RAGE: role on AOPPs-HSA-induced ROS generation. (**A**) Microplate wells were coated with 10 μg/ml of AOPPs-HSA, CML-HSA, GA-HSA, or native HSA. After washing and blocking, the wells were incubated with indicated concentrations of sRAGE. The bound sRAGE was detected with a HRP-conjugated monoclonal α-RAGE IgG. (**B**) CML-HSA (10 μg/ml) was immobilized onto the wells. sRAGE (4 μg/ml) was pre-incubated with indicated concentrations of AOPPs-HSA, CML-HSA, GA-HSA, or native HSA, and then added to the wells. The binding of sRAGE with immobilized AGEs-HSA was detected as described in **A**. (**C**) HUVECs were pre-incubated with a polyclonal α-RAGE IgG, a nonimmune IgG, or excess sRAGE, and then stimulated with AOPPs-HSA. ROS generation was determined by measuring the DCF fluorescence. (**D**) AOPPs-HSA (200 μg/ml) was pre-incubated with indicated concentrations of an α-AOPPs or a nonimmune IgG, and then interacted with HUVECs. ROS generation was determined as described above (*lower panel*). The α-AOPPs recognized AOPPs-HSA in Western blot (*upper panel, lane 1*), but did not react with CML- (*lane 2*), GA- (*lane 3*), GC- (*lane 4*), and RB-derived AGEs (*lane 5*) or native HSA (*lane 6*). (**E**) AOPPs-HSA was pre-incubated with indicated concentrations of 6D12 antibody and then interacted with HUVECs. ROS generation was measured as described above. (**F**) 6D12 antibody reacted with CML, GA- and GC-derived AGEs, and, to a lesser extent, with RB-derived protein. Data from three independent experiments are shown as mean ± SEM. ANOVA, $p < 0.001$ in **A**, **B**, and **C**; $p < 0.05$ in **D**. *$p < 0.05$ *vs.* wells coated with CML-HSA; #$p < 0.05$ *vs.* wells coated with AOPPs-HSA; §$p < 0.05$ *vs.* group pre-incubated with CML-HSA; II $p < 0.05$ *vs.* group pre-incubated with AOPPs-HSA; Δ $p < 0.05$ *vs.* group without respective inhibitors.

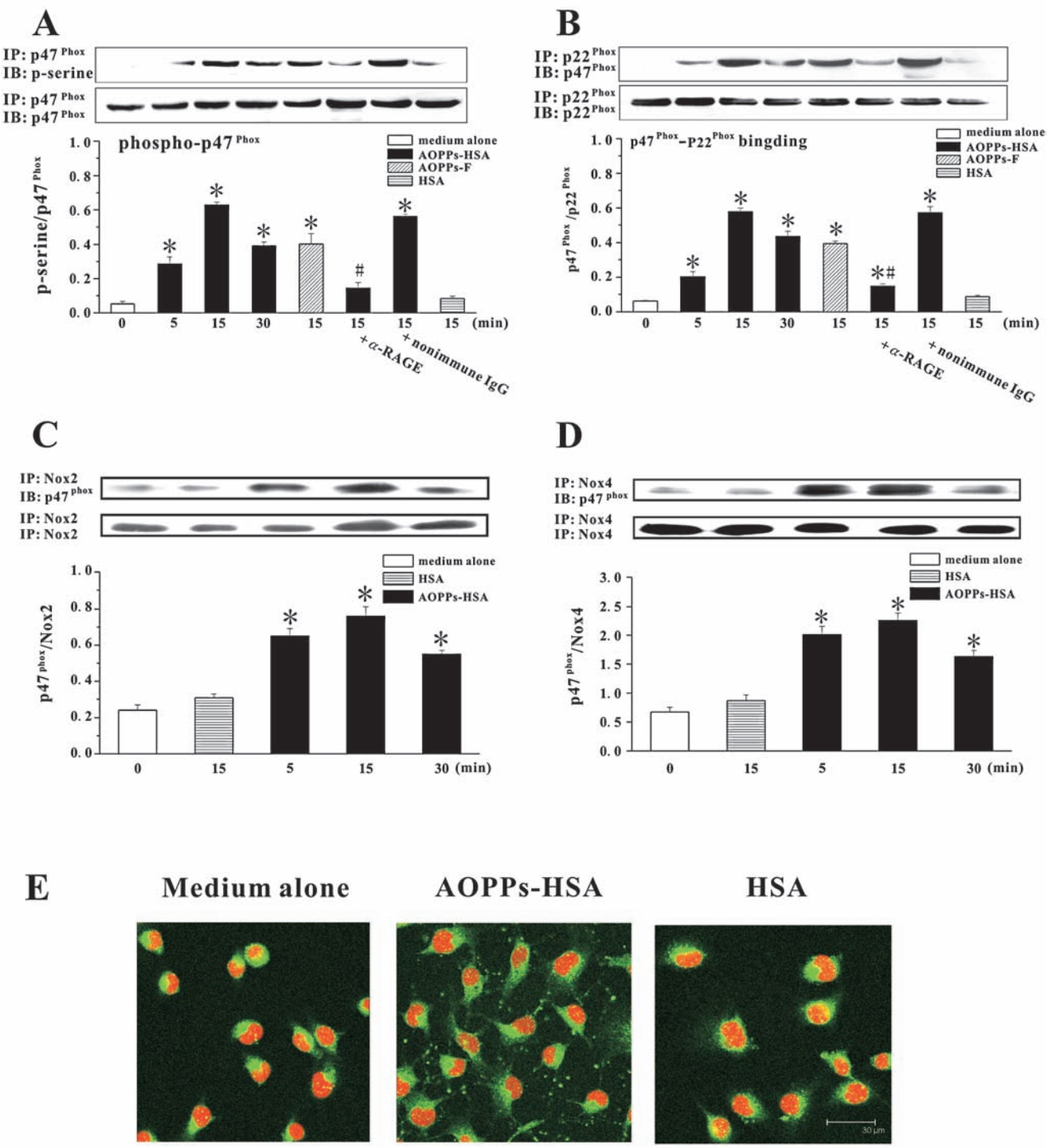

FIG. 3. AOPPs-induced activation of ECs NAD(P)H oxidase. (**A**) HUVECs were incubated with 200 μg/ml of AOPPs-HSA, AOPPs-F, or native HSA for 15~30 min. In some experiments, cells were pre-incubated with an α-RAGE IgG, a PKC inhibitor (Gö6983), or a nonimmune IgG and then stimulated with AOPPs-HSA. Phosphorylation of p47^{phox} was assayed by immunoprecipitation (IP) using an α-p47^{phox} and detected by immunoblotting (IB) using an α-pan-p47^{phox} and an α-phosphoserine as the primary antibodies. (**B**) AOPPs-induced binding of p47^{phox} to p22^{phox}. HUVECs were treated as described above. IP was performed by using an α-p22^{phox} and IB was conducted by using an α-p47^{phox}. (**C**) Interaction of p47^{phox} with Nox 2. HUVECs were treated as described above. IP was performed by using an α-Nox 2 and IB was conducted by using an α-p47^{phox}. (**D**) Interaction of p47^{phox} with Nox 4. HUVECs were treated as described above. IP was performed by using an α-Nox 4 and IB was conducted by using an α-p47^{phox}. (**E**) Representative photos of AOPPs-induced membrane translocation of p47^{phox}. HUVECs were incubated with an α-p47^{phox} and then with a FITC-conjugated α-mouse immunoglobulin and staining with PI. Data from three independent experiments are shown as mean ± SEM. ANOVA, $p < 0.001$ in **A** and **B**; *$p < 0.05$ as compared with groups treated with medium alone or HSA; #$p < 0.05$ *vs.* group without respective inhibitors. (For interpretation of the references to color in this figure legend, the reader is referred to the web version of this article at www.liebertonline.com/ars).

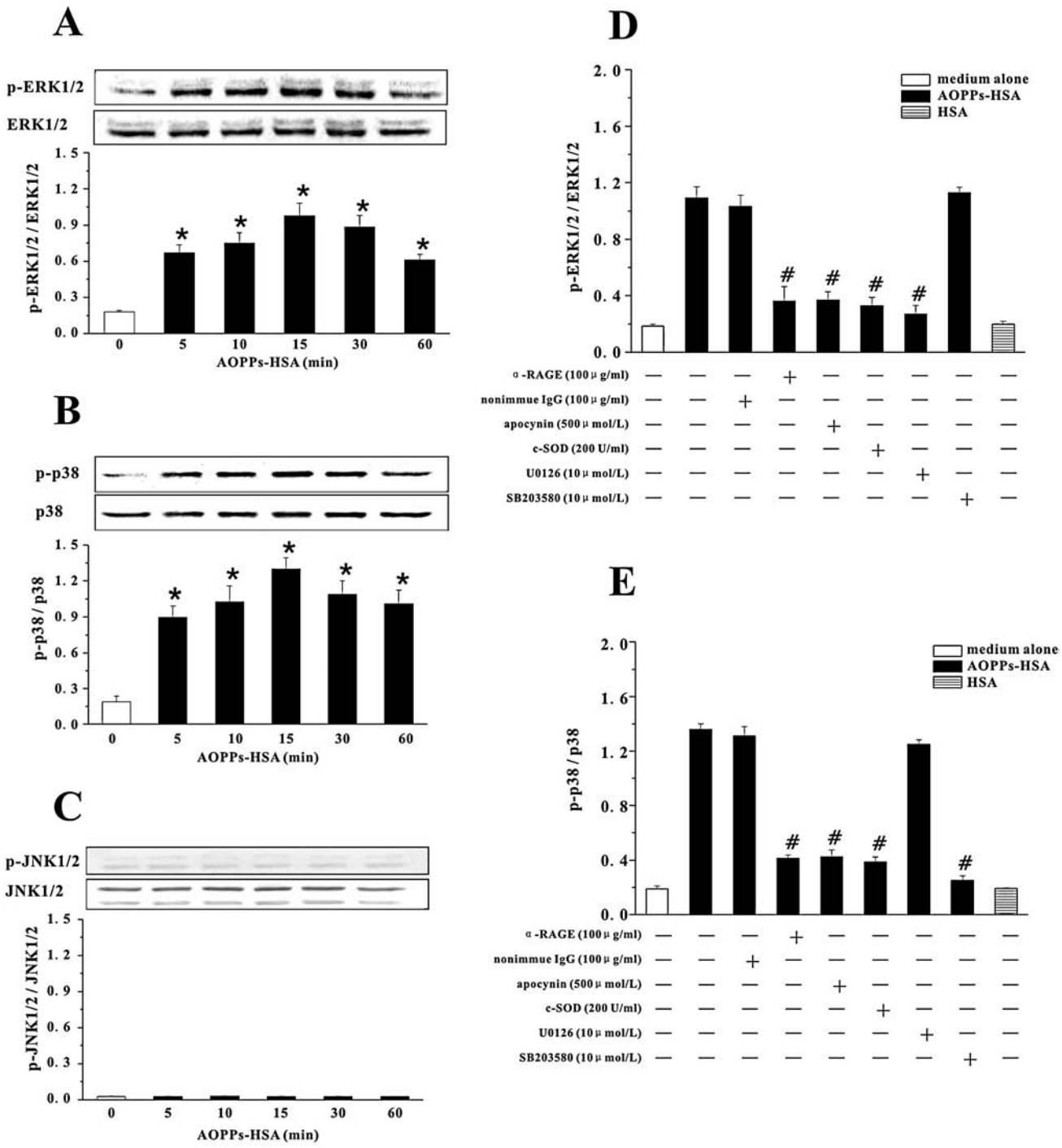

FIG. 4. AOPPs-HSA-induced MAPK activation in HUVECs. HUVECs were incubated with 200 μg/ml of AOPPs-HSA for indicated time. Phospho-ERK 1/2 (p-ERK 1/2) and ERK 1/2 (**A**), phospho-p38 (p-p38) and p38 (**B**), and phospho-JNK 1/2 (p-JNK 1/2) and JNK 1/2 (**C**) were detected by immunoblotting. In other experiments, HUVECs were pre-incubated with the α-RAGE IgG or nonimmune IgG, apocynin, c-SOD, or U0126/SB 203580. AOPPs-induced activation of ERK 1/2 (**D**) or p38 (**E**) was determined by immunoblotting. Data from three independent experiments are shown as mean ± SEM. ANOVA, $p < 0.001$ in **A**, **B**, **D**, and **E,** and $p = 1.000$ in **C**; *$p < 0.05$ as compared with groups treated with medium alone or HSA; #$p < 0.05$ *vs.* group without respective inhibitors.

NF-κB complex included mainly p65 and p50 (Fig. 5C). Competition experiments using unlabeled NF-κB or control Oct2A oligonucleotide probes demonstrated the specificity of the protein/DNA interaction (Fig. 5C).

To understand whether NF-κB activation depends on RAGE-mediated signals, we pretreated HUVECs with anti-RAGE IgG, apocynin, c-SOD, U0126/SB203580. All of these treatments inhibited AOPPs-HSA-induced p65 translocation (Fig. 5D) but had no effect on cells cultured in medium alone (data not shown), suggesting that AOPPs-induced NF-κB activation is associated with RAGE-mediated signals.

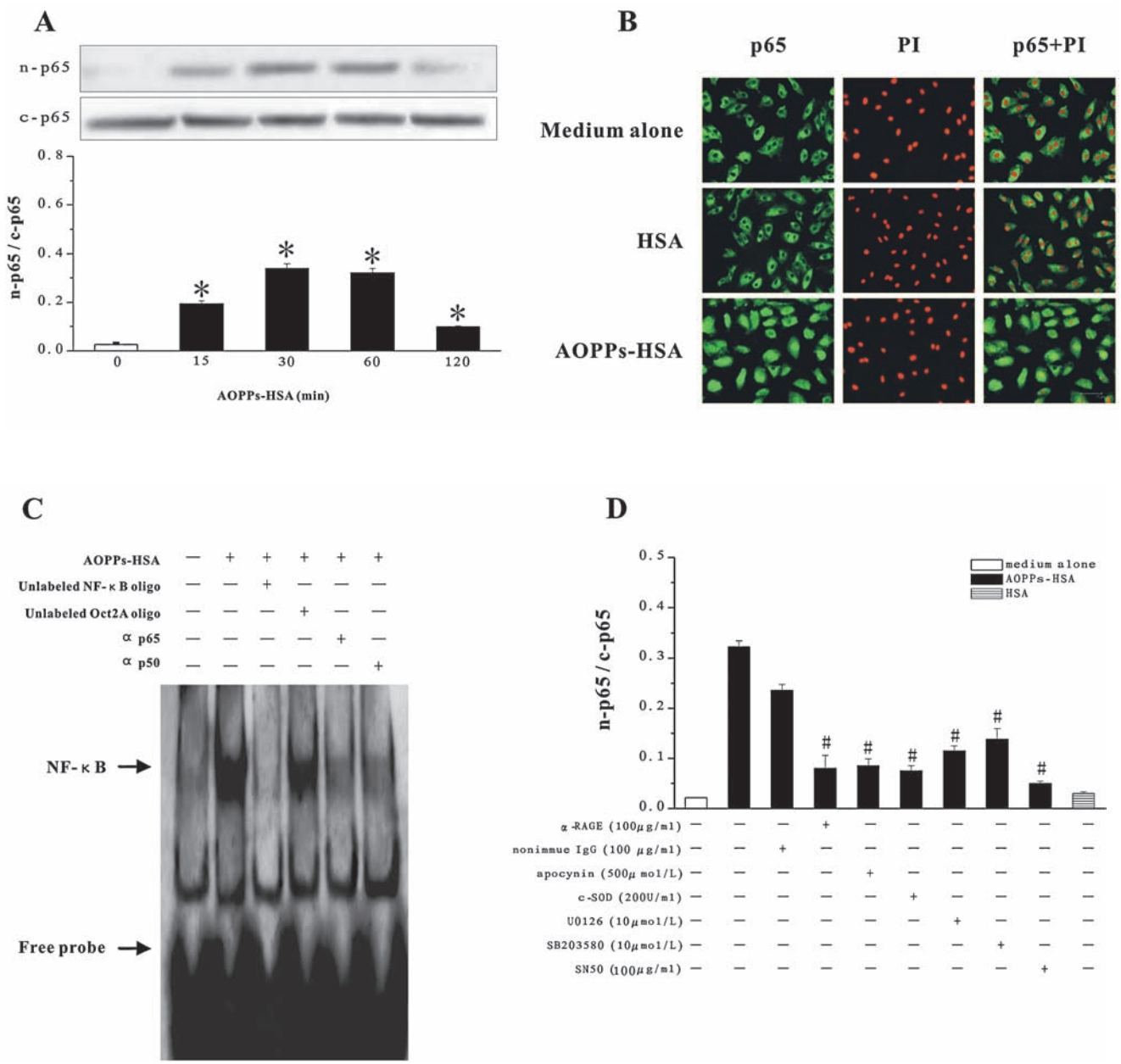

FIG. 5. AOPPs-induced NF-κB activation in HUVECs. (**A**) HUVECs were incubated with 200 μg/ml of AOPPs-HSA for indicated time. NF-κB p65 in the cytoplasmic extracts (c-p65) or in the nuclear extracts (n-p65) were detected by immunoblotting. (**B**) NF-κB p65 translocation was detected by immunofluorescence and PI staining. (**C**) NF-κB activation in nuclear extracts of AOPPs-HSA-stimulated HUVECs was detected by EMSA. (**D**) HUVECs were pretreated with the α-RAGE IgG or nonimmune IgG, apocynin, c-SOD, U0126/SB203580, and SN50 before AOPPs-HSA stimulation. The ratio of n-p65 and c-p65 was determined by immunoblotting. Data from three independent experiments are shown as mean ± SEM. ANOVA, $p < 0.001$ in **A** and **D**; *$p < 0.05$ as compared with group treated with medium alone; #$p < 0.05$ *vs.* group without respective inhibitors. (For interpretation of the references to color in this figure legend, the reader is referred to the web version of this article at www.liebertonline.com/ars).

FIG. 6. AOPPs-induced ICAM-1 and VCAM-1 expression in HUVECs. HUVECs were incubated with indicated concentrations of AOPPs-HSA for 6 h (**A**) or with 200 μg/ml of AOPPs-HSA for indicated time (**B**). ICAM-1 and VCAM-1 mRNA expression was measured by real time RT-PTCR. Expression of ICAM-1 and VCAM-1 protein was detected by immunoblotting (**C** and **D**). (**E**) Representative immunofluorescent staining for ICAM-1 and VCAM-1 in HUVECs. (**F** and **G**) HUVECs were pretreated with the α-RAGE IgG, apocynin, c-SOD, U0126/SB203580, and SN50. AOPPs-induced expression of ICAM-1 (**F**) and VCAM-1 (**G**) were determined by immunoblotting. Data from three independent experiments are shown as mean ± SEM. ANOVA, $p < 0.001$ in **A**, **B**, **C**, **D**, **F**, and **G**; *$p < 0.05$ as compared with group treated with medium alone; #$p < 0.05$ *vs.* group without respective inhibitors. (For interpretation of the references to color in this figure legend, the reader is referred to the web version of this article at www.liebertonline.com/ars).

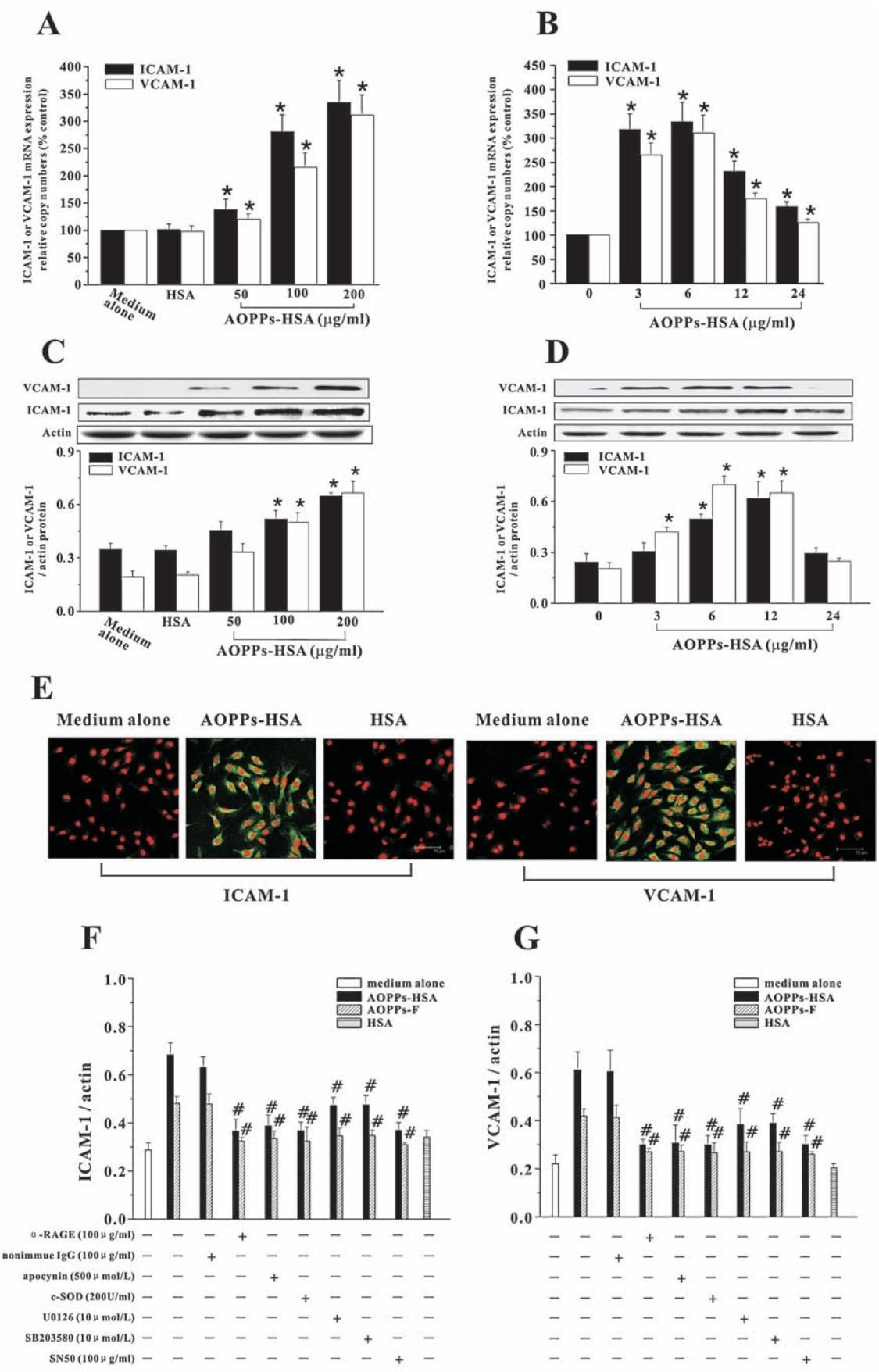
A
ICAM-1
VCAM-1
ICAM-1 or VCAM-1 mRNA expression relative copy numbers (% control)
Medium alone
HSA
50
100
200
AOPPs-HSA (μg/ml)
B
ICAM-1
VCAM-1
ICAM-1 or VCAM-1 mRNA expression relative copy numbers (% control)
0
3
6
12
24
AOPPs-HSA (μg/ml)
C
VCAM-1
ICAM-1
Actin
ICAM-1
VCAM-1
ICAM-1 or VCAM-1 / actin protein
Medium alone
HSA
50
100
200
AOPPs-HSA (μg/ml)
D
VCAM-1
ICAM-1
Actin
ICAM-1
VCAM-1
ICAM-1 or VCAM-1 / actin protein
0
3
6
12
24
AOPPs-HSA (μg/ml)
E
Medium alone
AOPPs-HSA
HSA
Medium alone
AOPPs-HSA
HSA
ICAM-1
VCAM-1
F
medium alone
AOPPs-HSA
AOPPs-F
HSA
ICAM-1 / actin
α-RAGE (100μg/ml)
nonimmue IgG (100μg/ml)
apocynin (500μmol/L)
c-SOD (200U/ml)
U0126 (10μmol/L)
SB203580 (10μmol/L)
SN50 (100μg/ml)
G
medium alone
AOPPs-HSA
AOPPs-F
HSA
VCAM-1 / actin

FIG. 6.

AOPPs induced ICAM-1 and VCAM-1 expression through RAGE-mediated signaling pathway

Expression of inducible adhesion molecules is a final common pathway in the development of vascular inflammation and can be modulated by ROS (30, 34). To investigate the potential impact of AOPPs-induced signaling pathway on adhesion molecules expression, we examined the effects of AOPPs-HSA or AOPPs-F on expression of ICAM-1 and VCAM-1. Exposure of HUVECs to AOPPs-HSA resulted in overexpression of ICAM-1 and VCAM-1 at both mRNA (Figs. 6A and B) and protein levels (Figs. 6C and D). Expression of ICAM-1 and VCAM-1 antigens was also enhanced in AOPPs-stimulated HUVECs as measured by immunofluorescence analysis (Fig. 6E). Overexpression of ICAM-1 (Fig. 6F) and VCAM-1 (Fig. 6G) were prevented by pretreatment of cells with apocynin, c-SOD, U0126/SB203580, or SN50, suggesting that AOPPs induced overexpression of adhesion molecules through NAD(P)H oxidase-ERK/p38-NF-κB signaling pathway.

To determine whether AOPPs effect through ligation of RAGE or other AGEs binding proteins, we examined expression of ICAM-1 and VCAM-1 in HUVECs pretreated with anti-RAGE IgG or other specific blocking antibodies against AGEs binding proteins. As shown in Fig. 6, pretreatment of HUVECs with anti-RAGE IgG prevented AOPPs-induced overexpression of adhesion molecules. However, the antibodies against other known AGEs binding proteins, at concentrations that block the interaction of AGEs with these binding proteins, were without effect (data not shown).

Discussion

Increased recognition of AOPPs, as a class of potential proinflammatory mediators and the multiple means by which they form in diverse disorders, has highlighted the importance of determining mechanisms by which AOPPs might modulate cellular properties. The present study demonstrated that AOPPs-albumin, either prepared *in vitro* or formed *in vivo*, bound to endothelial RAGE, induced ROS generation by activation of ECs NAD(P)H oxidase, and triggered a downstream signaling transduction involving ERK 1/2, p38 ^{MAPK}, and NF-κB. The cascade triggered by AOPPs resulted in overexpression of adhesion molecules such as ICAM-1 and VCAM-1. AOPPs-HSA, but not native HSA, activated the RAGE-dependent signals, suggesting that the triggering effect was due to AOPPs and not a property of HSA or other contaminants. For further confirmation, we isolated AOPPs from serum obtained from patients with uremia. The *in vivo* formed AOPPs exhibited biological activity in a manner similar with the *in vitro* prepared AOPPs. To the best of our knowledge, this is the first clarification of the proinflammatory pathway of AOPPs in ECs.

Exclusion of AGEs contamination in the AOPPs preparation is crucial. In our experimental setup, modification of HSA by HOCl was performed in the absence of free amino acids, and therefore no AGEs-like structures were formed (2, 24). Furthermore, we did not detect any significant level of CML and other AGEs structures in the AOPPs preparation. Third, the neutralizing anti-AGEs antibodies, at the concentrations that block the effect of CML-, GA-, GC- and RB-derived AGEs, could not inhibited $p47^{phox}$ phosphorylation and ROS generation, the major post-receptor upstream events induced by AOPPs. However, the anti-AOPPs antibody, which does not recognize any component of AGEs blocked ROS generation triggered by AOPPs. These data suggest that it seems unlikely to attribute the effect of AOPPs to AGEs contamination.

The most important finding in the present study is that AOPPs activated ECs by interaction with RAGE. RAGE is a member of the immunoglobulin superfamily of cell surface molecules (35), which interacts with multiple ligands, including AGEs, S100/calgranulins, amphoterin, and amyloid-β peptide (46). Interaction of AGEs with RAGE triggers an intracellular signaling pathway involving NADPH oxidase, MAPK, and NF-κB activation, leading to vascular perturbation and inflammation (19, 34, 35, 42). Since the first description of AOPPs,(43) its difference and identity with AGEs have been an issue of argument, because the two classes of modified proteins are sharing common features in biological activities and clinical indices (15, 43, 46), and because they are both composed of heterogeneous sets of compounds whose chemical structures have not been fully determined. The present study provided several lines of evidence demonstrating that AOPPs act as novel functional ligands for endothelial RAGE. First, AOPPs bound to sRAGE in a dose-dependent and saturable manner and competitively inhibited the binding of sRAGE with its preferential ligands AGEs. Second, AOPPs elicit a series of biochemical events in ECs which are similar with the consequences when RAGE is engaged by a signaling ligand, namely, PKC-associated O_2^- generation (38), activation of NADPH oxidase (42), ERK 1/2, $p38^{MAPK}$, and NF-κB (29), and induction of cell adhesion molecules (5). Third, the signaling pathway and the functional consequence of AOPPs-ECs interaction could be prevented by an anti-RAGE IgG and excess sRAGE, suggesting that AOPPs-RAGE interaction might be a novel mechanism for ECs activation. These observations support the hypothesis that activation of RAGE is a common pathway that transduces signals from the diverse biochemical and molecular species, leading to propagation of inflammation and vascular perturbation (19, 46). The bioactive structure of AOPPs, which interact with RAGE, has not been defined yet and is in active study.

Although the intracellular signal transduction triggered by AOPPs appears to be similar with that activated by AGEs, the *in vitro* binding affinity of AOPPs to RAGE was significantly higher than that of CML, a ligand of RAGE *in vivo* (46). The biological relevance of the difference between the two classes of modified albumin is unclear and is in active study. In fact, our recent observation has found that AOPPs exhibit higher capacity for promoting cellular inflammation and atherogenesis than CML-HSA in hyperlipidemic rabbits (data not published).

Another new finding of the study is that AOPPs-induced O_2^- is generated by a NADPH oxidase containing $p22^{phox}$, Nox 2, and Nox 4. AOPPs induced $p47^{phox}$ phosphorylation and its membrane translocation in HUVECs. The binding of $p47^{phox}$ to $p22^{phox}$ serves as a switch for activation of Nox 2 and Nox 4 (37, 41). HUVECs express Nox 2 and Nox 4, but not Nox 1 and Nox 3 (40). Nox 2 has been shown to be involved in O_2^- formation in several cells, including vascular endothelial cells (31). Although little is known about the function of Nox 4, there is evidence indicating that Nox 4 may also be involved in redox-mediated signal transduction in endothelial cells (1).

In contrast to oxidized lipids, the impact of oxidized proteins in vascular disease has not been extensively studied. The present report showed that AOPPs activated ECs *via* a

RAGE-mediated signaling pathway. AOPPs are prevalent in diverse pathophysiological conditions such as diabetes, renal insufficiency, and coronary artery disease, in which enhanced oxidative stress favors oxidative protein damage and, therefore, AOPPs formation (15, 43). Thus, identification of the molecular basis underlying AOPPs-induced ECs activation, possibly linked to the accelerated vascular disease observed in these disorders, might be a central step toward understanding the pathobiological effect of AOPPs and may provide targets for intervention.

Conclusions

We identified AOPPs as new functional ligands of RAGE in ECs. AOPPs activated vascular ECs through a RAGE-mediated signaling.

Acknowledgments

This work was supported by a National 973 program (No. 2006 CD 503904), a National Nature and Science Grant (No. 30330300) to Dr. Fan Fan Hou and a National Nature and Science Grant (No. 30600289) to Dr. Zhi Jian Guo.

Abbreviations

AGE-R, AGEs receptor; AGEs, advanced glycation end productis; AOPPs, advanced oxidation protein products; AOPPs-F, high-molecular-weight AOPPs fraction; AOPPs-HSA, AOPPs modified human serum albumin; CML, N^{ε}-(carboxylmethyl) lysine; CPS, counts per second; c-p65, cytoplasmic extracts; c-SOD, cytoplasmic superoxide dismutase; DCF, 5 (and 6)-chloromethyl-2′, 7′-dichlorodrofluorescein diacetate; DPI, diphenyleneiodonium; HOCl, hypochlorous acid; L-NAME, N^{G}-nitro-L-arginine methyl ester; Lox-1, lectin-like oxidized low-density lipoprotein receptor-1; n-p65, nuclear extracts; p-ERK 1/2, Phospho-ERK 1/2; p-JNK 1/2, phospho-JNK 1/2; PI, propidium iodide; p-p38, phospho-p38; RAGE, receptor for AGEs; SR-AI, scavenger receptor class A type 1; SR-BI, scavenger receptor class B type 1; sRAGE, extracellular domain of RAGE; SR-E1, scavenger receptor class E type 1; SREC-1, scavenger receptor expressed by ECs; SR-F1, scavenger receptor class F type 1;

References

1. Ago T, Kitazono T, Ooboshi H, Iyama T, Han YH, Takada J, Wakisaka M, Ibayashi S, Utsumi H, and Iida M. Nox4 as the major catalytic component of an endothelial NAD(P)H oxidase. *Circulation* 109: 227–233, 2004.
2. Anderson MM, Requena JR, Crowley JR, Thorpe SR, and Heinecke JW. The myeloperoxidase system of human phagocytes generates Nepsilon-(carboxymethyl)lysine on proteins: a mechanism for producing advanced glycation end products at sites of inflammation. *J Clin Invest* 104: 103–113, 1999.
3. Atabek ME, Keskin M, Yazici C, Kendirci M, Hatipoglu N, Koklu E, and Kurtoglu S. Protein oxidation in obesity and insulin resistance. *Eur J Pediatr* 165: 753–756, 2006.
4. Bass DA, Parce JW, Dechatelet LR, Szejda P, Seeds MC, and Thomas M. Flow cytometric studies of oxidative product formation by neutrophils: a graded response to membrane stimulation. *J Immunol* 130: 1910–1917, 1983.
5. Basta G, Lazzerini G, Massaro M, Simoncini T, Tanganelli P, Fu C, Kislinger T, Stern DM, Schmidt AM, and De Caterina R. Advanced glycation end products activate endothelium through signal-transduction receptor RAGE: a mechanism for amplification of inflammatory responses. *Circulation* 105: 816–822, 2002.
6. Capeillere–Blandin C, Gausson V, Scamps–Latscha B, and Witko–Sarsat V. Biochemical and spectrophotometric significance of advanced oxidized protein products. *Biochim Biophys Acta* 1689: 91–102, 2004.
7. Delanian S, Martin M, Bravard A, Luccioni C, and Lefaix JL. Cu/Zn superoxide dismutase modulates phenotypic changes in cultured fibroblasts from human skin with chronic radiotherapy damage. *Radiother Oncol* 58: 325–331, 2001.
8. Drueke T, Witko–Sarsat V, Massy Z, Scamps–Latscha B, Guerin AP, Marchais SJ, Gausson V, and London GM. Iron therapy, advanced oxidation protein products, and carotid artery intima-media thickness in end-stage renal disease. *Circulation* 106: 2212–2217, 2002.
9. Hazell LJ, Arnold L, Flowers D, Waeg G, Malle E, and Stocker R. Presence of hypochlorite-modified proteins in human atherosclerotic lesions. *J Clin Invest* 97: 1535–1544, 1996.
10. Horiuchi S, Sakamoto Y, and Sakai M. Scavenger receptors for oxidized and glycated proteins. *Amino Acids* 25: 283–292, 2003.
11. Hou FF. Cardiovascular risk in Chinese patients with chronic kidney diseases: where do we stand? *Chin Med J (Engl)* 118: 883–886, 2005.
12. Hou FF, Miyata T, Boyce J, Yuan Q, Chertow GM, Kay J, Schmidt AM, and Owen WF. beta(2)-Microglobulin modified with advanced glycation end products delays monocyte apoptosis. *Kidney Int* 59: 990–1002, 2001.
13. Jersmann HP, Hii CS, Ferrante JV, and Ferrante A. Bacterial lipopolysaccharide and tumor necrosis factor alpha synergistically increase expression of human endothelial adhesion molecules through activation of NF-kappaB and p38 mitogen-activated protein kinase signaling pathways. *Infect Immun* 69: 1273–1279, 2001.
14. Kaji Y, Usui T, Oshika T, Matsubara M, Yamashita H, Araie M, Murata T, Ishibashi T, Nagai R, Horiuchi S, and Amano S. Advanced glycation end products in diabetic corneas. *Invest Ophthalmol Vis Sci* 41: 362–368, 2000.
15. Kalousova M, Skrha J, and Zima T. Advanced glycation end-products and advanced oxidation protein products in patients with diabetes mellitus. *Physiol Res* 51: 597–604, 2002.
16. Kaneda H, Taguchi J, Ogasawara K, Aizawa T, and Ohno M. Increased level of advanced oxidation protein products in patients with coronary artery disease. *Atherosclerosis* 162: 221–225, 2002.
17. Kobayashi S, Suzuki M, Tsuneki H, Nagai R, Horiuchi S, and Hagino N. Overproduction of N(epsilon)-(carboxymethyl) lysine-induced neovascularization in cultured choroidal explant of streptozotocin-diabetic rat. *Biol Pharm Bull* 27: 1565–1571, 2004.
18. Krolewski AS, Warram JH, Valsania P, Martin BC, Laffel LM, and Christlieb AR. Evolving natural history of coronary artery disease in diabetes mellitus. *Am J Med* 90: 56S–61S, 1991.
19. Lander HM, Tauras JM, Ogiste JS, Hori O, Moss RA, and Schmidt AM. Activation of the receptor for advanced glycation end products triggers a p21(ras)-dependent mitogen-activated protein kinase pathway regulated by oxidant stress. *J Biol Chem* 272: 17810–17814, 1997.
20. Li HY, Hou FF, Zhang X, Chen PY, Liu SX, Feng JX, Liu ZQ, Shan YX, Wang GB, Zhou ZM, Tian JW, and Xie D. Advanced oxidation protein products accelerate renal fibrosis in a remnant kidney model. *J Am Soc Nephrol* 18: 528–538, 2007.
21. Li JM, Mullen AM, Yun S, Wientjes F, Brouns GY, Thrasher AJ, and Shah AM. Essential role of the NADPH oxidase subunit p47(phox) in endothelial cell superoxide production in response to phorbol ester and tumor necrosis factor-alpha. *Circ Res* 90: 143–150, 2002.

22. Li JM and Shah AM. Mechanism of endothelial cell NADPH oxidase activation by angiotensin II. Role of the p47phox subunit. *J Biol Chem* 278: 12094–12100, 2003.
23. Li T, Chen YH, Liu TJ, Jia J, Hampson S, Shan YX, Kibler D, and Wang PH. Using DNA microarray to identify Sp1 as a transcriptional regulatory element of insulin-like growth factor 1 in cardiac muscle cells. *Circ Res* 93: 1202–1209, 2003.
24. Liu SX, Hou FF, Guo ZJ, Nagai R, Zhang WR, Liu ZQ, Zhou ZM, Zhou M, Xie D, Wang GB, and Zhang X. Advanced oxidation protein products accelerate atherosclerosis through promoting oxidative stress and inflammation. *Arterioscler Thromb Vasc Biol* 26: 1156–1162, 2006.
25. Livak KJ and Schmittgen TD. Analysis of relative gene expression data using real-time quantitative PCR and the 2(-delta delta C(T)) method. *Methods* 25: 402–408, 2001.
26. Marsche G, Heller R, Fauler G, Kovacevic A, Nuszkowski A, Graier W, Sattler W, and Malle E. 2-chlorohexadecanal derived from hypochlorite-modified high-density lipoprotein-associated plasmalogen is a natural inhibitor of endothelial nitric oxide biosynthesis. *Arterioscler Thromb Vasc Biol* 24: 2302–2306, 2004.
27. Menon V, Gul A, and Sarnak MJ. Cardiovascular risk factors in chronic kidney disease. *Kidney Int* 68: 1413–1418, 2005.
28. Nagai R, Hayashi CM, Xia L, Takeya M, and Horiuchi S. Identification in human atherosclerotic lesions of GA-pyridine, a novel structure derived from glycolaldehyde-modified proteins. *J Biol Chem* 277: 48905–48912, 2002.
29. Nah SS, Choi IY, Yoo B, Kim YG, Moon HB, and Lee CK. Advanced glycation end products increases matrix metalloproteinase-1, -3, and -13, and TNF-alpha in human osteoarthritic chondrocytes. *FEBS Lett* 581: 1928–1932, 2007.
30. Nakashima Y, Raines EW, Plump AS, Breslow JL, and Ross R. Upregulation of VCAM-1 and ICAM-1 at atherosclerosis-prone sites on the endothelium in the ApoE-deficient mouse. *Arterioscler Thromb Vasc Biol* 18: 842–851, 1998.
31. Petry A, Djordjevic T, Weitnauer M, Kietzmann T, Hess J, and Gorlach A. NOX2 and NOX4 mediate proliferative response in endothelial cells. *Antioxid Redox Signal* 8: 1473–1484, 2006.
32. Reddy S, Bichler J, Wells–Knecht KJ, Thorpe SR, and Baynes JW. N epsilon- (carboxymethyl)lysine is a dominant advanced glycation end product (AGE) antigen in tissue proteins. *Biochemistry* 34: 10872–10878, 1995.
33. Sady C, Jiang CL, Chellan P, Madhun Z, Duve Y, Glomb MA, and Nagaraj RH. Maillard reactions by alpha-oxoaldehydes: detection of glyoxal-modified proteins. *Biochim Biophys Acta* 1481: 255–264, 2000.
34. Schmidt AM, Hori O, Chen JX, Li JF, Crandall J, Zhang J, Cao R, Yan SD, Brett J, and Stern D. Advanced glycation endproducts interacting with their endothelial receptor induce expression of vascular cell adhesion molecule-1 (VCAM-1) in cultured human endothelial cells and in mice. A potential mechanism for the accelerated vasculopathy of diabetes. *J Clin Invest* 96: 1395–1403, 1995.
35. Schmidt AM, Vianna M, Gerlach M, Brett J, Ryan J, Kao J, Esposito C, Hegarty H, Hurley W, and Clauss M. Isolation and characterization of two binding proteins for advanced glycosylation end products from bovine lung which are present on the endothelial cell surface. *J Biol Chem* 267: 14987–14997, 1992.
36. Shan YX, Yang TL, Mestril R, and Wang PH. Hsp10 and Hsp60 suppress ubiquitination of insulin-like growth factor-1 receptor and augment insulin-like growth factor-1 receptor signaling in cardiac muscle: implications on decreased myocardial protection in diabetic cardiomyopathy. *J Biol Chem* 278: 45492–45498, 2003.
37. Sumimoto H, Ueno N, Yamasaki T, Taura M, and Takeya R. Molecular mechanism underlying activation of superoxide-producing NADPH oxidases: roles for their regulatory proteins. *Jpn J Infect Dis* 57: S24–S25, 2004.
38. Thallas–Bonke V, Thorpe SR, Coughlan MT, Fukami K, Yap FY, Sourris K, Penfold S, Bach LA, Cooper ME, and Forbes JM. Inhibition of NADPH oxidase prevents AGE mediated damage in diabetic nephropathy through a protein kinase C-{alpha} dependent pathway. *Diabetes* 57: 460–469, 2008.
39. Valencia JV, Weldon SC, Quinn D, Kiers GH, DeGroot J, TeKoppele JM, and Hughes TE. Advanced glycation end product ligands for the receptor for advanced glycation end products: biochemical characterization and formation kinetics. *Anal Biochem* 324: 68–78, 2004.
40. Van Buul JD, Fernandez–Borja M, Anthony EC, and Hordijk PL. Expression and localization of NOX2 and NOX4 in primary human endothelial cells. *Antioxid Redox Signal* 7: 308–317, 2005.
41. Van Heerebeek L, Meischl C, Stooker W, Meijer CJ, Niessen HW, and Roos D. NADPH oxidase(s): new source(s) of reactive oxygen species in the vascular system? *J Clin Pathol* 55: 561–568, 2002.
42. Wautier MP, Chappey O, Corda S, Stern DM, Schmidt AM, and Wautier JL. Activation of NADPH oxidase by AGE links oxidant stress to altered gene expression via RAGE. *Am J Physiol Endocrinol Metab* 280: E685–E694, 2001.
43. Witko–Sarsat V, Friedlander M, Capeillere–Blandin C, Nguyen–Khoa T, Nguyen AT, Zingraff J, Jungers P, and Scamps-Latscha B. Advanced oxidation protein products as a novel marker of oxidative stress in uremia. *Kidney Int* 49: 1304–1313, 1996.
44. Witko–Sarsat V, Gausson V, Nguyen AT, Touam M, Drueke T, Santangelo F, and Scamps–Latscha B. AOPP-induced activation of human neutrophil and monocyte oxidative metabolism: a potential target for N-acetylcysteine treatment in dialysis patients. *Kidney Int* 64: 82–91, 2003.
45. Yan SD, Schmidt AM, Anderson GM, Zhang J, Brett J, Zou YS, Pinsky D, and Stern D. Enhanced cellular oxidant stress by the interaction of advanced glycation end products with their receptors/binding proteins. *J Biol Chem* 269: 9889–9897, 1994.
46. Yan SF, Ramasamy R, Naka Y, and Schmidt AM. Glycation, inflammation, and RAGE: a scaffold for the macrovascular complications of diabetes and beyond. *Circ Res* 93: 1159–1169, 2003.
47. Zhu P, Tang L, Zhao SC, Lu X, Hou FF, and Fu N. Preparation of monoclonal antibodies against different epitopes on extracellular domain of human receptor for advanced glycation end product. *Di Yi Jun Yi Da Xue Xue Bao* 24: 129–132, 2004.
48. Zund G, Uezono S, Stahl GL, Dzus AL, McGowan FX, Hickey PR, and Colgan SP. Hypoxia enhances induction of endothelial ICAM-1: role for metabolic acidosis and proteasomes. *Am J Physiol* 273: C1571–C1580, 1997.

Address reprint requests to:
Dr. Fan Fan Hou
Division of Nephrology
Nanfang Hospital
Southern Medical University
1838 North Guangzhou Avenue
Guangzhou, 510515
P. R. China

E-mail: ffhou@public.guangzhou.gd.cn

Date of first submission to ARS Central, December 3, 2007; date of final revised submission, April 10, 2008; date of acceptance, April 12, 2008.